




Article

Elastocaloric Effect in Aged Single Crystals of Ni₅₄Fe₁₉Ga₂₇ Ferromagnetic Shape Memory Alloy

Elena Y. Panchenko , Eleonora I. Yanushonite, Anna S. Eftifeeva, Aida B. Tokhmetova, Irina D. Kurlevskaya, Anton I. Tagiltsev , Nikita S. Surikov , Ekaterina E. Timofeeva and Yuri I. Chumlyakov

Laboratory for Physics of High-Strength Crystals, Siberian Physical-Technical Institute, Tomsk State University, Lenin Avenue 36, 634050 Tomsk, Russia

* Correspondence: panchenko@mail.tsu.ru

Abstract: In the present study, the effect of γ' -phase dispersed particles on both the L2₁(B2)-10M/14M-L1₀ martensitic transformations and the elastocaloric effect in aged Ni₅₄Fe₁₉Ga₂₇ single crystals oriented along the [001]-direction was investigated. It was experimentally shown that aging strongly affects the elastocaloric properties of these crystals. The precipitation of semi-coherent γ' -phase particles up to 500 nm in size in the crystals aged at 773 K for 1 h leads to a 1.4 times increase in the operating temperature range of the elastocaloric effect up to $\Delta T_{SE} = 270$ K as compared with the initial as-grown crystals ($\Delta T_{SE} = 197$ K). The adiabatic cooling values ΔT_{ad} are similar for the as-grown crystals $\Delta T_{ad} = 10.9 (\pm 0.5)$ K and crystals aged at 773 K $\Delta T_{ad} = 11.1 (\pm 0.5)$ K. The crystals containing incoherent γ' -phase particles sized 5–35 μm (after aging at 1373 K for 0.5 h) possess an operating temperature range of $\Delta T_{SE} = 255$ K with slightly smaller adiabatic cooling ΔT_{ad} below 9.7 (± 0.5) K. The aged [001]-oriented Ni₅₄Fe₁₉Ga₂₇ single crystals demonstrate high cyclic stability: the number of cycles does not influence the adiabatic cooling values and parameters of loading/unloading curves regardless of the particle size. The ways to improve the elastocaloric cooling parameters and stability of the elastocaloric effect by means of dispersed particles in the NiFeGa ferromagnetic shape memory alloy were discussed.

Keywords: martensitic transformation; elastocaloric effect; dispersed particles; single crystals; ferromagnetic shape memory alloy



Citation: Panchenko, E.Y.; Yanushonite, E.I.; Eftifeeva, A.S.; Tokhmetova, A.B.; Kurlevskaya, I.D.; Tagiltsev, A.I.; Surikov, N.S.; Timofeeva, E.E.; Chumlyakov, Y.I. Elastocaloric Effect in Aged Single Crystals of Ni₅₄Fe₁₉Ga₂₇ Ferromagnetic Shape Memory Alloy. *Metals* **2022**, *12*, 1398. <https://doi.org/10.3390/met12081398>

Academic Editors: Yan Feng and Li Gao

Received: 14 July 2022

Accepted: 16 August 2022

Published: 22 August 2022

Publisher's Note: MDPI stays neutral with regard to jurisdictional claims in published maps and institutional affiliations.



Copyright: © 2022 by the authors. Licensee MDPI, Basel, Switzerland. This article is an open access article distributed under the terms and conditions of the Creative Commons Attribution (CC BY) license (<https://creativecommons.org/licenses/by/4.0/>).

1. Introduction

Developing eco-friendly materials for solid-state cooling systems is a promising solution to the global warming problem. The main operating principle of solid-state cooling systems is based on the caloric effect that is associated with a reversible change in the entropy or temperature of a solid body caused by the influence of external fields (electric E, magnetic H, mechanical σ , or hydrostatic pressure P) under isothermal or adiabatic conditions, respectively. New materials should possess significant cooling capability, high reliability, stability, and durability, as well as satisfy the economic requirements in order to be used as efficient solid-state cooling systems [1,2].

Shape memory alloys (SMAs) are widely used for engineering such devices because of the promising elastocaloric effect (EC effect). The EC effect is accompanied by a giant value of adiabatic cooling up to 31.5 K per working cycle [3]. Moreover, it is easier to create conditions for the implementation of the EC effect during loading/unloading cycles in SMAs than in magneto-caloric or electro-caloric materials.

Ferromagnetic NiFeGa-based SMAs with L2₁(B2)-10M/14M-L1₀ martensitic transformations (MTs) are one of the most promising materials possessing functional properties required for solid-state cooling systems. Single crystals of such SMAs are characterized by a wide superelasticity (SE) temperature interval, which is also the working range of the EC effect. To date, the EC effect has been studied only in as-grown NiFeGa single

crystals without additional heat treatments. It was shown that the best properties were found in high-strength crystals oriented along the $[001]_{L2_1}$ -direction: adiabatic cooling ΔT_{ad} reaches 8.4–9.8 K for one loading/unloading cycle with narrow stress hysteresis in a wide temperature range of 190–200 K in compression [4–7].

Improving functional properties in NiFeGa crystals by aging is a topical task. Improvements will strengthen materials, expand a working temperature range, and ensure high cyclic stability of functional properties. It is known that the precipitation of $\gamma(\gamma')$ -phase particles with the face-centered lattice or ordered $L1_2$ -structure occurs in NiFeGa SMAs after austenite aging [8–10]. Thus, aging in austenite enables the creation of heterophase crystals whose matrix undergoes thermoelastic MT, whereas precipitated dispersed particles do not undergo MT, they act as elastic elements that store elastic energy, and they contribute to the development of reversible thermoelastic MT. It is assumed that, in aged NiFeGa alloys containing dispersed particles, necessary conditions will be created to obtain the wide operating temperature range and high cyclic stability of the EC effect. It should be noted that the precipitation of $\gamma(\gamma')$ -phase particles in $Ni_{49}Fe_{18}Ga_{27}Co_6$ and $CoNiAl$ single crystals decreases stress hysteresis, increases the SE temperature interval, and improves the SE cyclic stability [9–12].

According to the above-mentioned, the aim of the present study is to find out the effect of particles precipitated after austenite aging on the SE and the EC effect in $Ni_{54}Fe_{19}Ga_{27}$ single crystals oriented along the $[001]$ -direction. Along this direction, the theoretical value of the compressive transformation strain for $L2_1(B2)$ - $L1_0$ MT is the maximum value of 6.2% [13]. Moreover, this high-strength $[001]$ -orientation is characterized by the absence of detwinning of $L1_0$ -martensite under compressive stress because of the zero Schmid factors for the $L1_0$ -martensite twinning system. In this case, the SE is accompanied by the minimal value of dissipative energy and stress hysteresis $\Delta\sigma$ in comparison with the other orientations ($[011]$, $[123]$), where the detwinning of $L1_0$ -martensite occurs under compressive stress [13–16]. Therefore, the $[001]$ -direction provides optimal conditions for observing both the SE and the EC effect in studied crystals.

2. Materials and Methods

The single crystals of $Ni_{54}Fe_{19}Ga_{27}$ (at. %) alloy were grown by Bridgman method in an inert gas atmosphere. For compression testing parallelepiped samples with dimensions of $3 \times 3 \times 6 \text{ mm}^3$ were cut using an electrical-discharge machine ARTA 123 (Delta-Test, Moscow, Russia). The compression axis corresponds to the long side of a sample and possesses the $[001]$ -orientation in austenite. The orientation of single crystals in $L2_1(B2)$ -austenite was defined by a DRON-3 X-ray diffractometer (Burevesnik, St. Petersburg, Russia) using FeK α radiation.

Two aged single crystals were studied in the present research:

- aged at 773 K for 1 h followed by slow air cooling in order to keep the austenite $L2_1$ -structure (after aging at 773 K);
- aged at 1373 K for 0.5 h followed by quenching in water.

Such a choice of thermal treatments will allow varying the particle size and austenite structure [8–10] in order to create a different degree of particle coherency with austenite and martensite and to study the influence of particle size to EC effect. To compare and find out the effect of dispersed particles on both the EC effect and stress-induced MT, the previously obtained results [17] on the initial $[001]_A$ -oriented $Ni_{54}Fe_{19}Ga_{27}$ single crystals were used.

Transformation temperatures of $L2_1(B2)$ -10M/14M- $L1_0$ MT are defined by differential scanning calorimetry (DSC) method using a DSC 404 F1 Pegasus calorimeter (NETZSCH, Bayern, Germany). Temperature M_s , M_f for forward and A_s , A_f for reverse transformation, changes in the entropy ΔS and specific heat capacity at constant pressure C_p were established according to the standard methods after DSC studies, as it was shown in [18].

SE was studied along the [001]-compression axis using an Instron VHS 5969 universal testing machine (Instron, High Wycombe, UK); the instrumental error is ± 2 MPa. The adiabatic temperature change ΔT_{ad} in the single crystals was defined by direct measurement using a highly-sensitive T-type thermal couple (RS International, Northamptonshire, UK) fixed on the sample surface. The mechanical experiments with the EC effect measurement were arranged as follows: first, the sample was loaded with a low strain rate of $2.0 \times 10^{-3} \text{ s}^{-1}$ until the given stress was reached; then, the sample was kept at that stress level for about 10 s in order to equalize the sample temperature; the following unloading was performed with a high strain rate of $6.7 \times 10^{-1} \text{ s}^{-1}$ to create the conditions close to adiabatic. The instrumental error for ΔT_{ad} during the EC effect is ± 0.5 K. The data on the change in the sample temperature depending on the test time is recorded by the data acquisition module along with the data on the stress change and strain depending on the test time. This allows us to accurately match two datasets and to establish $\sigma(\epsilon)$ and $\Delta T_{ad}(t)$ dependences. Transmission electron microscopic studies (TEM) were performed in Krasnoyarsk Science Center SB RAS on transmission electron microscope HT-7700 Hitachi (Hitachi, Tokyo, Japan).

3. Results

The microstructure of the $\text{Ni}_{54}\text{Fe}_{19}\text{Ga}_{27}$ crystals after austenite aging at 773 K and 1373 K was examined using TEM. It is shown that aging results in the precipitation of γ' -phase particles having the ordered $L1_2$ crystal structure (Figures 1 and 2).

Aging at 773 K for 1 h leads to the precipitation of γ' -phase particles with the size of 170–500 nm (Figure 1). The particles have the ordered $L1_2$ crystal structure, which is confirmed by the superlattice reflections of 100 and 110 (Figure 1c). The precipitated particles have an elongated or close to equilateral shape. It is assumed that such particles are semi-coherent. The assumption is confirmed by both the strain contrast near particles and the absence of dislocations at the interphase boundary.

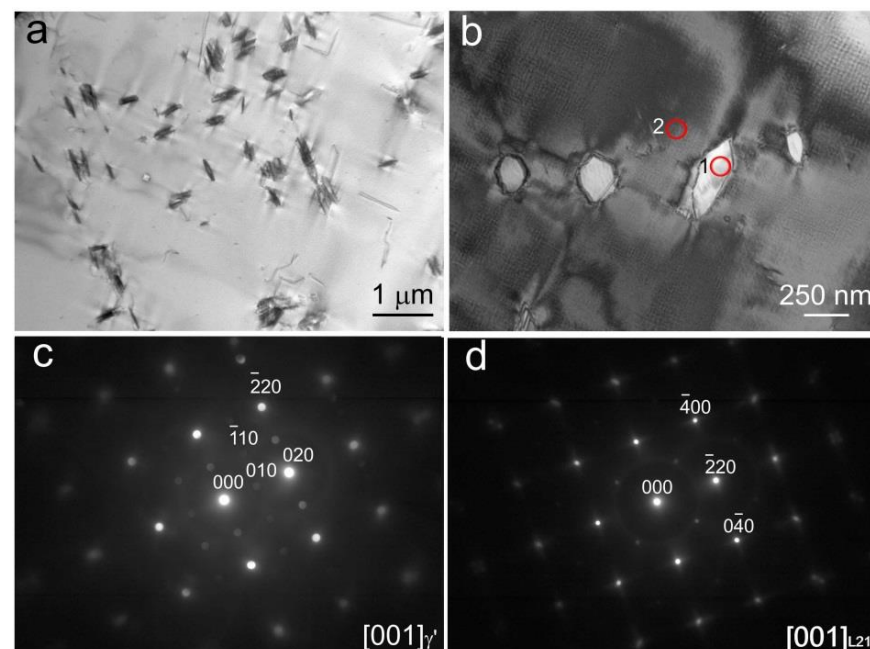


Figure 1. TEM image of the microstructure in the $\text{Ni}_{54}\text{Fe}_{19}\text{Ga}_{27}$ single crystals aged at 773 K for 1 h: bright field (BF) image of matrix and particles (a,b) and the selected area diffraction patterns from γ' -phase particles with the ordered $L1_2$ structure (area 1 is indicated in b) (c) and $L2_1$ -austenite, zone axis $[001]_{L2_1}$ (area 2 is indicated in b) (d).

Figure 2 shows the microstructure of the $\text{Ni}_{54}\text{Fe}_{19}\text{Ga}_{27}$ single crystals aged at 1373 K for 0.5 h. There are large incoherent particles with the size of 5–35 μm and volume fraction of $(24 \pm 5)\%$ in these crystals. It should be noted that the high density of dislocations is observed at the particle–matrix boundary. As mentioned above, the superlattice reflections of 100 and 110 are the evidence of the ordered L_{12} crystal structure in such particles. Some of γ' -phase particles have an elliptical shape and consist of two parts connected by twinning relation (Figure 2c,d), which is consistent with the previous study [19]. The transformation temperatures as well as the heat parameters of MT for all studied $\text{Ni}_{54}\text{Fe}_{19}\text{Ga}_{27}$ single crystals were defined by DSC method (Figure 3, Table 1). The single crystals aged at 773 K for 1 h are characterized by lower transformation temperatures as compared with the as-grown crystals or crystals aged at 1373 K, which demonstrate the highest temperatures. The decrease in the MT temperatures in the crystals aged at $T = 773$ K can occur due to an increase in the degree of order of the high-temperature phase, the effects of dispersion strengthening, and an increase in the elastic and surface energies necessary to maintain the compatibility of the martensitic deformation of the matrix and the elastic deformation of the γ' -phase particles. The increase in the MT temperatures in the crystals aged at 1373 K, firstly, is caused by the change from L_{21} to B2 in the austenite structure. This is in accordance with the previously obtained results [6,20,21]: changes in the austenite structure from L_{21} -phase to B2-phase in the NiFeGa alloy occur at 933–978 K. Secondly, the dislocation formation near large γ' -phase particles (Figure 2d), as well as the changing chemical composition of the matrix during the precipitation of large γ' -phase particles (for example the decrease in Fe component by 2 at.%) increases the transformation temperatures [22].

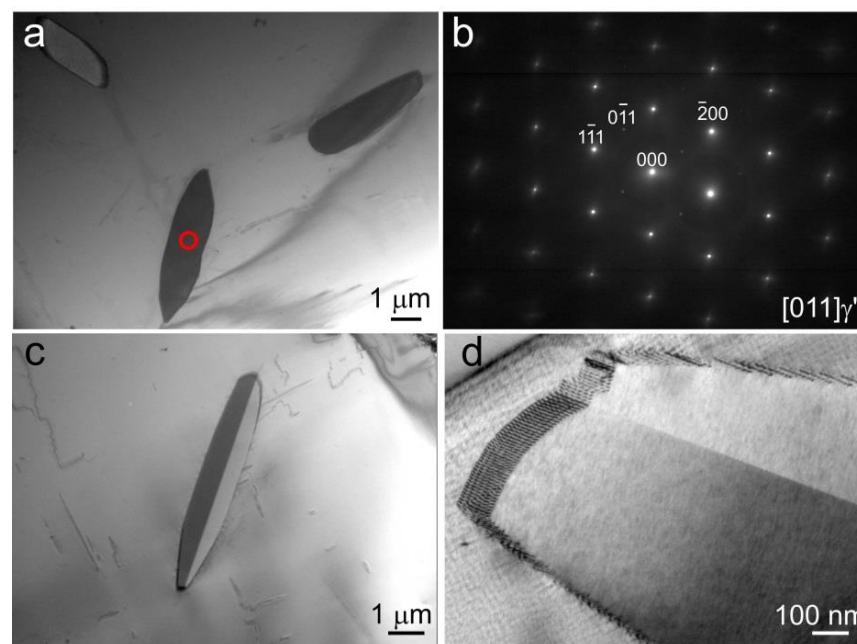


Figure 2. TEM image of the microstructure in the $\text{Ni}_{54}\text{Fe}_{19}\text{Ga}_{27}$ single crystals aged at 1373 K for 0.5 h: BF image of matrix and particles (a–c) and the selected area diffraction patterns (area is indicated in (a)) from γ' -phase particles with an ordered L_{12} structure (d).

Table 1. Characteristic parameters of MT and heat characteristics from DSC response for [001]-single crystals $\text{Ni}_{54}\text{Fe}_{19}\text{Ga}_{27}$.

Heat Treatment	$M_s, (\pm 2)$ K	$M_f, (\pm 2)$ K	$A_s, (\pm 2)$ K	$A_f, (\pm 2)$ K	$C_p, \text{J}/(\text{kgK})$	$\Delta S^{A-M}, \text{J}/(\text{kgK})$	$\Delta S^{M-A}, \text{J}/(\text{kgK})$	$\Delta T_{ad}^{t(A-M)}, \text{K}$	$\Delta T_{ad}^{t(M-A)}, \text{K}$
As-grown [17]	276	265	280	289	488	−17.6	16.5	10.2	9.6
Aged at 773 K	259	245	257	270	434	−15.9	14.2	9.7	8.7
Aged at 1373 K	281	261	274	295	418	−14.0	10.1	9.6	7.0

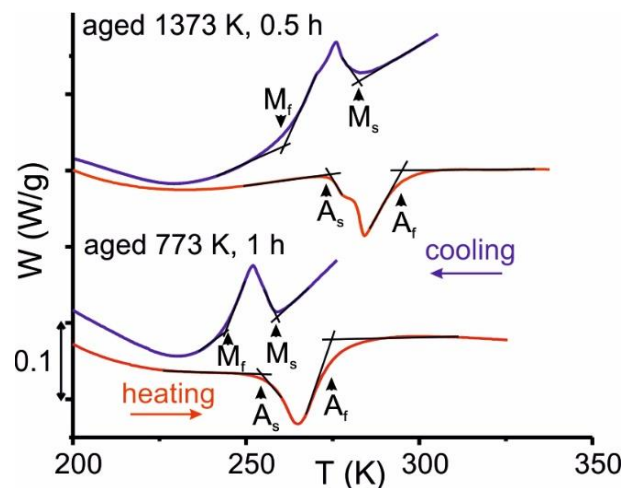


Figure 3. DSC curves for aged [001]-oriented $\text{Ni}_{54}\text{Fe}_{19}\text{Ga}_{27}$ single crystals.

It is experimentally shown that the precipitation leads to a decrease in the magnitude of the change in entropy ΔS^{A-M} (ΔS^{M-A}) during both forward and reverse MT (Table 1). It is mainly associated with the increase in the volume fraction of particles that do not undergo transformations. Therefore, the volume of the material undergoing MT decreases. The specific heat capacity C_p also decreases by 54 J/(kgK) in the crystals aged at 773 K and by 70 J/(kgK) in the crystals aged at 1373 K in comparison with the as-grown crystals (Table 1).

Based on the experimental data, it is possible to estimate the maximum theoretical value of adiabatic cooling ΔT_{ad} during the manifestation of the EC effect [6]:

$$\Delta T_{ad} \approx \frac{T_0 \Delta S}{C_p}, \quad (1)$$

where C_p —specific heat capacity, ΔS —entropy change, $T_0 \approx 1/2(M_s + A_f)$ —equilibrium temperature between austenite and martensite phases.

Theoretical values of the adiabatic temperature change ΔT_{ad} obtained from DSC assume a small decrease in ΔT_{ad} by 1–2 K in the aged crystals in comparison with the as-grown ones.

The stress–strain curves at different temperatures in loading/unloading cycles and corresponding sample temperature change for the [001]-oriented $\text{Ni}_{54}\text{Fe}_{19}\text{Ga}_{27}$ single crystals aged at 773 K for 1 h and 1373 K for 0.5 h are shown in Figure 4. For each test temperature, the red line shows a change in the sample temperature during loading, the blue line shows a change in the sample temperature during unloading. The adiabatic cooling ΔT_{ad} was measured during loading/unloading cycles under the SE conditions at different test temperatures. The maximum applied stress level was 800 MPa in each cycle at the test temperature from A_f to 473 K. In the studied crystals, the EC effect is also observed at $T > 473$ K, but to complete the stress-induced MT it is necessary to increase the applied stresses above 800 MPa.

The obtained experimental data show that the working temperature range and the EC cooling in the $\text{Ni}_{54}\text{Fe}_{19}\text{Ga}_{27}$ single crystals depend on the aging temperature.

The single crystals aged at 773 K demonstrate a wide SE and EC effect temperature range $\Delta T_{SE} = 270$ K (from 278 to 548 K), which is 1.4 times greater compared with the as-grown crystals ($\Delta T_{SE} = 197$ K, from 298 up to 493 K) [17]. This wide temperature range is facilitated, on the one hand, by the lower temperature $A_f = 270$ K (Table 1). On the other hand, in the crystals aged at 773 K, a higher dislocation slip resistance is observed during the stress-induced MT. The resistance is higher because of the hardening of the matrix by γ' -phase dispersed particles, which expands the SE and EC effect temperature range towards high temperatures. The temperature, at which the irreversible strain more than 0.5% was observed on the $\sigma(\epsilon)$ curves, was taken as the end temperature of the SE range.

In these crystals, aged at 773 K for 1 h, the EC cooling value reaches $\Delta T_{ad} = 11.1 (\pm 0.5)$ K at the test temperature $T = 296$ K (Figure 4a).

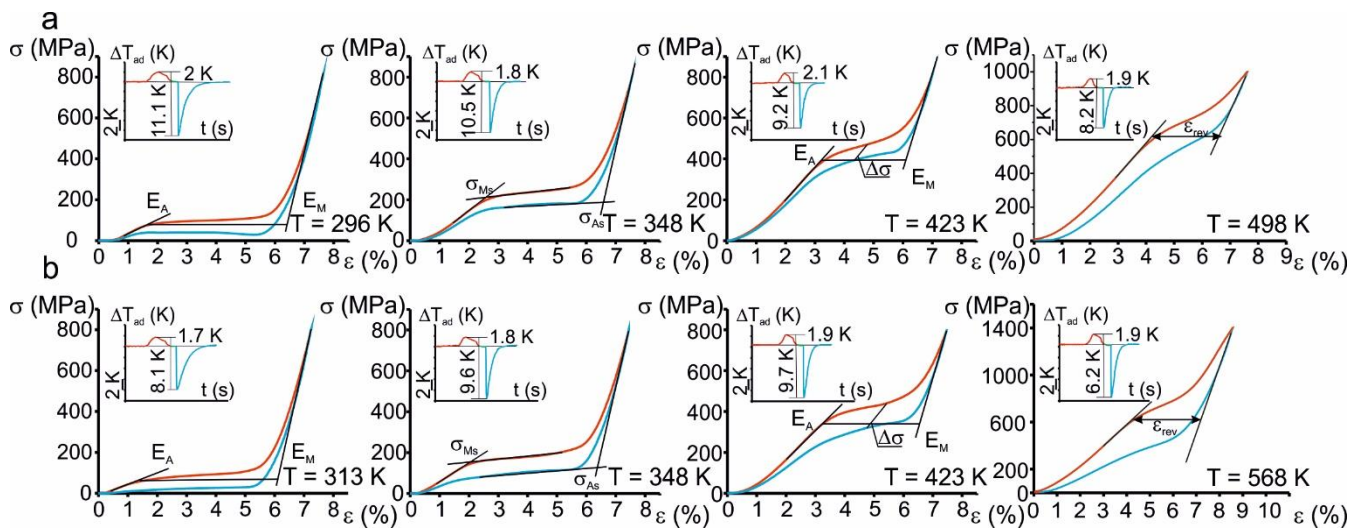


Figure 4. SE curves and corresponding thermograms at different test temperatures for [001]-oriented $\text{Ni}_{54}\text{Fe}_{19}\text{Ga}_{27}$ single crystals aged at 773 K for 1 h (a) and aged at 1373 K for 0.5 h (b).

In the single crystals undergoing high-temperature aging at 1373 K, the MT temperatures increase due to the precipitation of incoherent γ' -phase particles, which leads to narrowing of the SE temperature range $\Delta T_{SE} = 255$ K (from 313 to 568 K) as compared with low-temperature aging at 773 K. The single crystals aged at 1373 K are characterized by wider stress hysteresis because of the presence of a large volume fraction of incoherent γ' -phase particles in the material that do not undergo MT and the stored elastic energy can relax due to plastic deformation of the particles during the forward MT (Figure 4b).

4. Discussion

It has been experimentally established that in the single crystals aged at 773 K for 1 h, the maximum EC cooling value $\Delta T_{ad} = 11.1$ K is observed. The single crystals with incoherent particles aged at 1373 K for 0.5 h are characterized by the lower maximum values of $\Delta T_{ad} = 9.7$ K as compared with the crystals aged at 773 K. A decrease in the ΔT_{ad} value with an increase in the γ' -phase particle size was predicted using the DSC data (Table 1). However, the maximum experimental ΔT_{ad} values slightly exceed the theoretical estimates of adiabatic cooling $\Delta T_{ad}^{t(M-A)}$ obtained from DSC (by 1.0–2.5 K). The theoretical values $\Delta T_{ad}^{t(M-A)}$ are usually greater than the experimental ones because the heat exchange of the sample with testing machine grips is always observed and experimental conditions are not strictly adiabatic.

This difference between the theoretical, i.e., calculated with the DSC data $\Delta T_{ad}^{t(M-A)}$ for the reverse MT (Table 1), and experimental EC cooling ΔT_{ad} values is determined by different staging and entropy change for thermal-induced and stress-induced MT in NiFeGa single crystals. It has been found that in the as-grown NiFeGa(Co) crystals [23–25], one-stage $L2_1$ -14M MT occurs and a self-accommodated structure of 14M martensite is formed during cooling/heating in the stress-free state. During the stress-induced MT, the growth of oriented $L1_0$ -martensite is observed and $L2_1$ -14M- $L1_0$ or $L2_1$ - $L1_0$ MT takes place. Therefore, the magnitude of the entropy change during the stress-induced MT can be estimated using the temperature dependence of the critical stresses $\sigma_{Ms}(T)$ or $\sigma_{As}(T)$ required for the onset of forward and reverse MT according to the Clausius–Clapeyron equation [17,26]:

$$\Delta S^{A-M} = \frac{\epsilon_{tr}}{\rho} \frac{d\sigma_{Ms}}{dT} \quad \text{and} \quad \Delta S^{M-A} = \frac{\epsilon_{tr}}{\rho} \frac{d\sigma_{As}}{dT} \quad (2)$$

where ε_{tr} is the transformation strain; $\rho = 8450 \text{ kg/m}^3$ —density [27].

Figure 5 shows the temperature dependence of the critical stresses of forward σ_{Ms} and reverse σ_{As} stress-induced MT. For the single crystals aged at 773 K, σ_{Ms} and σ_{As} stresses increase linearly with the test temperature. In contrast, a significant deviation of $\sigma_{As}(T)$ from the linear dependence is observed in the crystals aged at 1373 K at test temperature $T > 450 \text{ K}$.

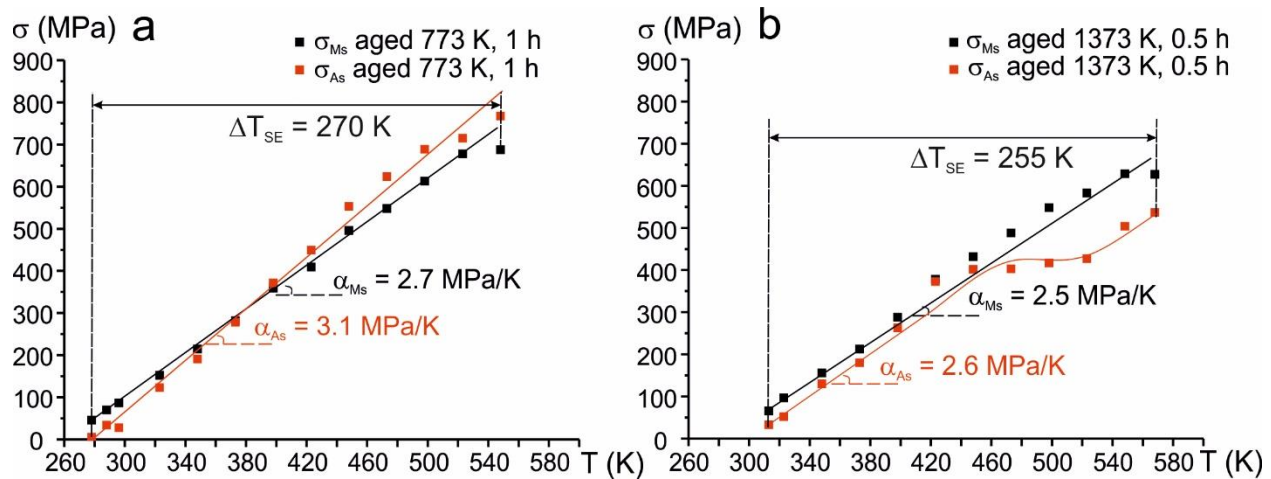


Figure 5. The temperature dependence of the critical stresses of forward σ_{Ms} and reverse σ_{As} MT for [001]-oriented $\text{Ni}_{54}\text{Fe}_{19}\text{Ga}_{27}$ single crystals aged at 773 K for 1 h (a) and at 1373 K for 0.5 h (b).

As it was shown in [17,28,29], the critical stresses for forward σ_{Ms} and reverse σ_{As} MT can be expressed as:

$$\sigma_{Ms}(T) = \sigma_0(T) + \rho \frac{|\Delta G_{dis}(0, T)| + |\Delta G_{rev}(0, T)|}{\varepsilon_{tr}(T)} \quad (3)$$

$$\sigma_{As}(T) = \sigma_0(T) - \rho \frac{|\Delta G_{dis}(0, T)| + |\Delta G_{rev}(0, T)|}{\varepsilon_{tr}(T)} \quad (4)$$

Here $\Delta G_{dis}(0, T)$, $\Delta G_{dis}(1, T)$, $\Delta G_{rev}(0, T)$, and $\Delta G_{rev}(1, T)$ are the dissipated and the stored elastic energy (reversible energy) per unit mass at the start (volume fraction $\delta = 0$) and at the end of ($\delta = 1$) stress-induced MT. If we assume that $\Delta G_{rev}(0, T)$ has small values and weakly depends on the test temperature, stress σ_0 can be defined as:

$$\sigma_0(T) = \frac{\sigma_{Ms} - \sigma_{As}}{2} \quad (5)$$

If the dissipation energy ΔG_{dis} and stored elastic energy ΔG_{rev} do not depend on temperature, the Clausius–Clapeyron slope for forward $\alpha_{Ms} = d\sigma_{Ms}/dT$ and reverse MT $\alpha_{As} = d\sigma_{As}/dT$ is similar. However, there is a strong temperature dependence of both dissipation ΔG_{dis} and stored elastic ΔG_{rev} energy in the temperature range of the EC effect in the studied aged single crystals. It is known [17,28,29] that the dissipation energy ΔG_{dis} is proportional to stress hysteresis $\Delta\sigma$ and the stored elastic energy ΔG_{rev} is proportional to the strain rate hardening $\theta = d\sigma/d\varepsilon$ during the stress-induced MT.

In the crystals aged at 773 K, the strain rate hardening $\theta = d\sigma/d\varepsilon$ and, accordingly, the stored elastic energy ΔG_{rev} increase with the test temperature. That is why, according to Equations (3) and (4), the Clausius–Clapeyron slope for reverse MT $\alpha_{As} = d\sigma_{As}/dT = 3.1 \text{ MPa/K}$ is higher than for the forward one MT $\alpha_{Ms} = d\sigma_{Ms}/dT = 2.7 \text{ MPa/K}$. A similar dependence was observed earlier for as-grown [001]-oriented crystals [17]. The elastic accommodation of austenite and martensite crystals becomes more difficult during the stress-induced MT with an increase in the test temperature. Therefore, at elevated test temperatures in the as-grown crystals and the crystals aged at 773 K, MT is accompanied

by high θ and significant accumulation of stored elastic energy $\Delta G_{\text{rev}}(1,T)$, which is the driving force of the reverse MT (Figure 4). As Figure 5 shows, at $T > 400$ K, the reverse MT begins at critical stresses σ_{As} higher than for the forward one σ_{Ms} . For the reverse MT, the temperature dependence of $\theta = d\sigma/d\varepsilon$ and $\Delta G_{\text{rev}}(1,T)$ leads to a sharper increase in critical stresses σ_{As} with the test temperature and, accordingly, to higher Clausius–Clapeyron slope $d\sigma_{\text{As}}/dT$ in comparison with the forward one (σ_{Ms} and $d\sigma_{\text{Ms}}/dT$).

The crystals with large incoherent γ' -phase particles aged at 1373 K are characterized by wide stress hysteresis $\Delta\sigma$, which is 2–4 times greater than for the as-grown crystals and crystals aged at 773 K and increases sharply at test temperatures $T > 450$ K (Figure 4). This leads to high energy dissipation $\Delta G_{\text{dis}}(1,T)$, and, in accordance with Equation (4), to a sharp decrease in σ_{As} at test temperatures $T > 450$ K (Figure 5).

The test temperature grows and alters the values of the stored elastic energy $\Delta G_{\text{rev}}(1,T)$ and the dissipated energy $\Delta G_{\text{dis}}(1,T)$. These changes contribute to the experimental $d\sigma_{\text{As}}/dT$ values and the $\Delta S^{\text{M-A}}$ values calculated with Equation (2). $d\sigma_{\text{As}}/dT$ can change sharply with an increase in the strain rate hardening $\theta = d\sigma/d\varepsilon$ or stress hysteresis $\Delta\sigma$ that also change with the test temperature. The conditions for the martensite nucleation and, accordingly, stored elastic $\Delta G_{\text{rev}}(0,T)$ and dissipated $\Delta G_{\text{dis}}(0,T)$ energy weakly depend on the test temperature. Thus, it is necessary to use α_{Ms} and $\Delta S^{\text{A-M}}$ for forward MT for entropy change during stress-induced MT and EC cooling $\Delta T_{\text{ad}}^{\text{t(A-M)}}$ estimations. The calculated values are shown in Table 2. It can be seen that there is good agreement between the theoretical and experimental values of the EC cooling.

Table 2. Maximum theoretical $\Delta T_{\text{ad}}^{\text{t(A-M)}}$, calculated by Equations (1) and (2), and experimental $\Delta T_{\text{ad}}^{\text{exp(max)}}$ EC effect values for $[001]_{\text{A}}$ -oriented $\text{Ni}_{54}\text{Fe}_{19}\text{Ga}_{27}$ single crystals.

Heat Treatment	α_{Ms} , MP/K	C_p , J/(kgK)	$ \varepsilon_{\text{rev}} ^{\text{max}}$, %	$\Delta S^{\text{A-M}}$, J/(kgK)	$\Delta T_{\text{ad}}^{\text{t(A-M)}}$, K	$\Delta T_{\text{ad}}^{\text{exp(max)}}$, K
Aged at 773 K	2.7	434	5.4	−17.2	10.5	11.1 (± 0.5)
Aged at 1373 K	2.5	418	4.7	−13.9	9.6	9.7 (± 0.5)

Figure 6 shows the temperature dependence of the adiabatic temperature change ΔT_{ad} , reversible strain, and stress hysteresis in the aged single crystals in comparison with the as-grown single crystals of the $\text{Ni}_{54}\text{Fe}_{19}\text{Ga}_{27}$ alloy. The aged crystals demonstrate the similar temperature dependences of the adiabatic temperature change ΔT_{ad} , which do not depend on the size of the dispersed γ' -phase particles (Figure 6a). There is an increase in ΔT_{ad} to the maximum values at the start of the SE temperature range. This $\Delta T_{\text{ad}}(T)$ dependence behavior is typical for many SMAs [6]. During the test temperature near A_f and the SE manifestation, the sample is locally cooled by ΔT_{ad} to temperature below A_f . This can inhibit the reverse MT and reduce the ΔT_{ad} . Therefore, the maximum adiabatic temperature change ΔT_{ad} is reached at the test temperature $T \geq A_f + \Delta T_{\text{ad}}(\text{max})$. Then almost constant ΔT_{ad} is achieved in the temperature interval of 50–75 K (Figure 6a). After that, unlike the as-grown crystals, the aged crystals see ΔT_{ad} decrease linearly with the increasing temperature. In the as-grown crystals, a weak temperature dependence of ΔT_{ad} in the operating temperature range is observed (Figure 6a).

In the aged crystals, both the adiabatic temperature change ΔT_{ad} and transformation strain ε_{rev} decrease with an increase in the test temperature (Figure 6a,b). The maximum transformation strain ε_{rev} at SE in the single crystals aged at 773 K is equal to $\varepsilon_{\text{rev}} = 5.4 (\pm 0.3)\%$. The reversible strain decreases by 2.2 times with an increase in the test temperature in the SE temperature window ($\varepsilon_{\text{rev}} = 2.3\%$ at $T = 548$ K). The maximum reversible strain at the SE is less ($\varepsilon_{\text{rev}} = 4.7 (\pm 0.3)\%$) in the crystals aged at 1373 K than in the crystals aged at 773 K. This is associated with a large volume fraction of particles (up to 24%) that do not undergo the transformation. The ε_{rev} in these crystals also decreases by 1.6 times with an increase in the test temperature. At elevated test temperatures $T \geq 448$ K, ε_{rev} is equal to $3.0 (\pm 0.3)\%$ in the crystals aged at 1373 K (Figure 6b). Decreasing

transformation strain ε_{rev} associated with an increase in the test temperature is a distinguishing characteristic of [001]-oriented single crystals of ferromagnetic CoNiGa, CoNiAl, NiMnGa, and NiFeGa(Co) alloys [12,13,17,25,30]. The reason for this $\varepsilon_{\text{rev}}(T)$ dependence is the difference between the elastic moduli of austenite and martensite $E_A \neq E_M$ (Figure 4). This is discussed in detail in our previous work on as-grown [001]-oriented NiFeGa single crystals [17].

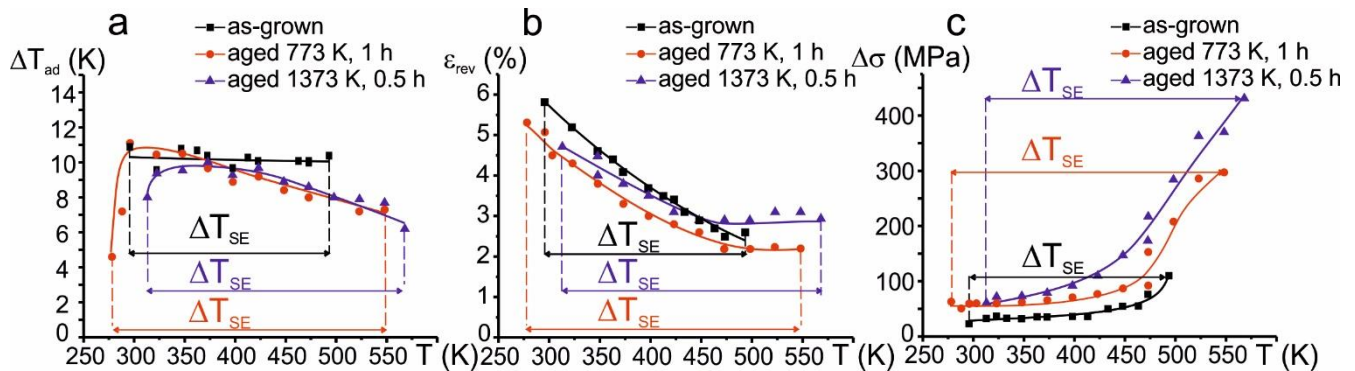


Figure 6. Temperature dependence of the adiabatic temperature change ΔT_{ad} (a), transformation reversible strain ε_{rev} (b), and stress hysteresis $\Delta\sigma$ (c) in loading/unloading cycles in [001]-oriented as-grown and aged Ni₅₄Fe₁₉Ga₂₇ single crystals.

A decreasing transformation strain associated with an increase in the test temperature is observed in both [001]-oriented as-grown and aged crystals. However, the adiabatic cooling ΔT_{ad} in the as-grown crystals remains constant with a decrease in transformation strain by 2.3–1.6 times [17]. Therefore, a decreasing transformation strain with an increase in temperature due to the difference between the elastic moduli of austenite and martensite cannot be the main reason for the ΔT_{ad} decrease in [001]-oriented aged NiFeGa crystals.

The γ' -phase precipitation leads to the two-fold increase in stress hysteresis $\Delta\sigma$ and, consequently, energy dissipation in the operating cycle in the aged crystals compared with the as-grown ones (Figure 6c). This is due to an increase in the friction force needed for the movement of the interphase boundary in the crystals containing dispersed particles, which do not undergo transformation. Stress hysteresis of $\Delta\sigma \approx 60$ –67 MPa in the single crystals aged at 773 K and of $\Delta\sigma \approx 34$ –40 MPa in the as-grown crystals are independent of the test temperature up to $T \approx 448$ K. The SE curves at temperature $T > 440$ K in the crystals aged at 773 K are characterized by irreversible strain of $\varepsilon_{\text{irr}} < 0.5\%$ and stress hysteresis increase from 87 MPa ($T = 448$ K) to 297 MPa ($T = 548$ K) (Figures 4 and 6c). The crystals with incoherent γ' phase particles aged at 1373 K are characterized by the maximum stress hysteresis $\Delta\sigma$ among the studied crystals. Stress hysteresis increases from 92 MPa to 431 MPa with the growth of the test temperature from $T = 398$ K to $T = 568$ K. A sharp increase in stress hysteresis also begins at the test temperature above 450 K in crystals aged at 773 K. Stress hysteresis generates from the energy dissipation not only in the form of frictional work to interfacial motion, but also in the form of plastic relaxation of the coherence stress in the martensite–austenite interface. The plastic relaxation of the coherence stress results in the irreversible strain ε_{irr} in loading/unloading. The analysis of the obtained experimental results shows that if there is no plastic relaxation of the coherence stress during MT, ΔT_{ad} weakly depends on stress hysteresis $\Delta\sigma$. However, if irreversible strain ε_{irr} is observed and stress-induced MT is accompanied by plastic accommodation in the working cycle, the ΔT_{ad} decreases with increasing $\Delta\sigma$. This is observed in the aged crystals at elevated test temperatures $T > 450$ K.

The energy dissipation in the operating cycle, which is proportional to stress hysteresis, is an important parameter for practical application and can have a significant influence on the cyclic stability of SE and EC effect. The cyclic stability of the SE and the EC effect in 150 loading/unloading cycles was studied in the crystals aged at 773 K at test

temperatures near $T = 323$ K and in the crystals aged at 1373 K at test temperatures near $T = 373$ K (Figures 7 and 8). This choice of test temperatures allows investigating the cyclic stability of the SE and the EC effect at similar critical stresses for martensite formation in these crystals. The maximum stress in the loading/unloading cycle was 600 MPa. It has been experimentally established that the aged [001]-oriented $\text{Ni}_{54}\text{Fe}_{19}\text{Ga}_{27}$ single crystals demonstrate high cyclic stability of the SE and the EC effect, which does not depend on the γ' phase particle size and stress hysteresis $\Delta\sigma$. An increase in the number of loading/unloading cycles, n from 1 to 150, does not affect the value of $\Delta T_{\text{ad}} = 9.0 (\pm 0.8)$ K (aged at 773 K for 1 h) and $\Delta T_{\text{ad}} = 8.5 (\pm 0.8)$ K (aged at 1373 K for 0.5 h).

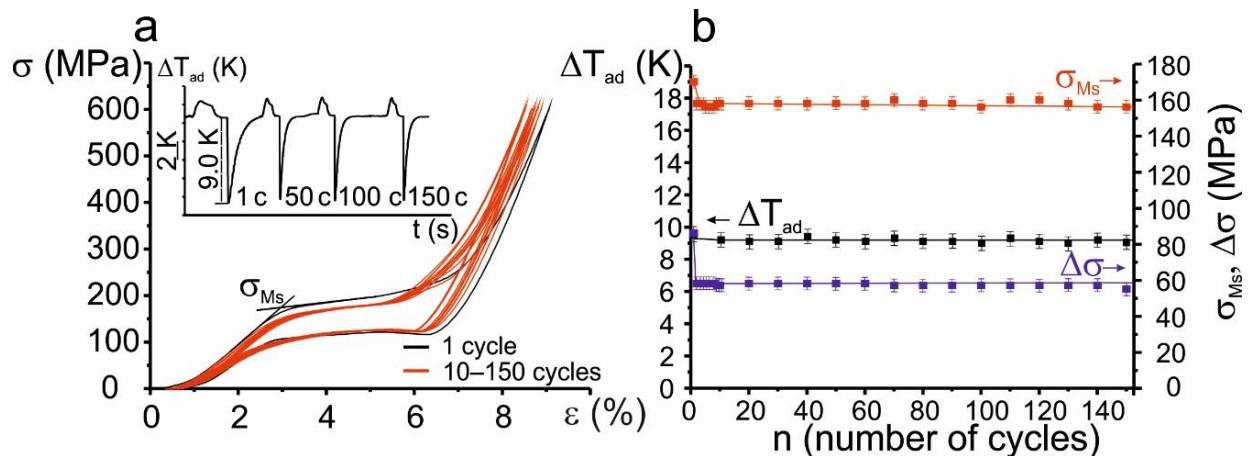


Figure 7. Compressive functional fatigue responses and EC fatigue at $T = 323$ K in aged at 773 K, 1 h $\text{Ni}_{54}\text{Fe}_{19}\text{Ga}_{27}$ single crystals, oriented along the [001]-direction: the dependence of SE curves with corresponding thermograms on number of cycles (a) and the dependence of adiabatic temperature change ΔT_{ad} , critical stresses of forward MT σ_{Ms} and stress hysteresis $\Delta\sigma$ on number of cycles (b).

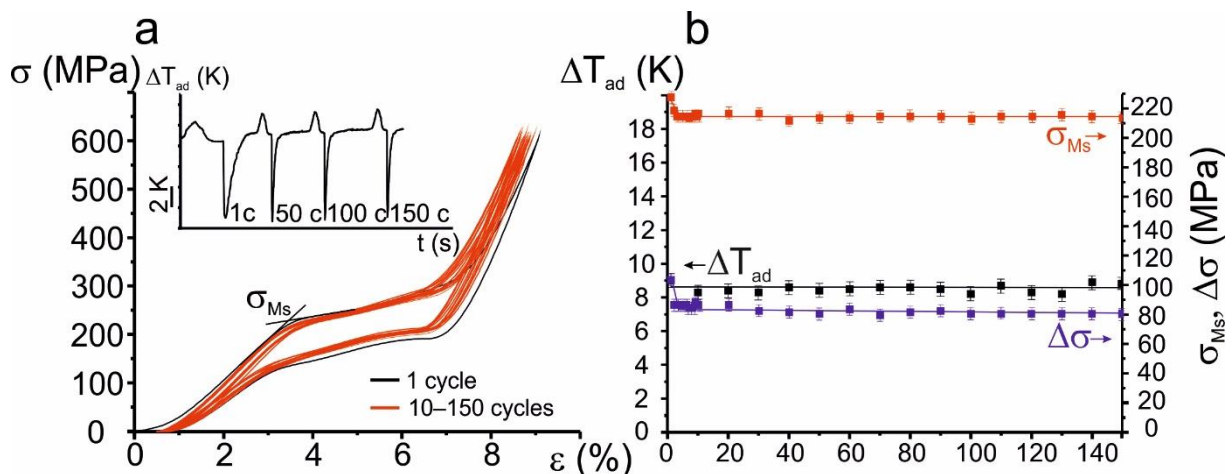


Figure 8. Compressive functional fatigue responses and EC fatigue at $T = 373$ K in aged 1373 K, 0.5 h $\text{Ni}_{54}\text{Fe}_{19}\text{Ga}_{27}$ single crystals oriented along the [001]_A-direction: the dependence of SE curves with corresponding thermograms on number of cycles (a) and the dependence of adiabatic temperature change ΔT_{ad} , critical stresses of forward MT σ_{Ms} and stress hysteresis $\Delta\sigma$ on number of cycles (b).

A degradation of the critical stresses of martensite formation σ_{Ms} and stress hysteresis $\Delta\sigma$ is observed only in the first three cycles, $n = 1-3$. The critical stresses σ_{Ms} go down by 12–13 MPa and stress hysteresis decreases by 20–28 MPa in the second cycle, $n = 2$, compared with $n = 1$ in the single crystals aged at 773 K and 1373 K. This is determined by the effect of the first cycle, which is accompanied by irreversible strain less than 0.5% in the first cycle and the formation of a small volume fraction of residual martensite and/or

dislocations. This contributes to the creation of favorable internal stress fields for the onset of stress-induced MT during the next cycles and a decrease in energy dissipation due to dislocation hardening, which leads to a decrease in σ_{Ms} and $\Delta\sigma$. Such an effect of the first cycle is the common characteristic of SMAs when SE occurs [31].

Thus, despite different stress hysteresis, both aged $\text{Ni}_{54}\text{Fe}_{19}\text{Ga}_{27}$ single crystals oriented along the [001]-direction and as-grown crystals demonstrate high cyclic stability of SE and EC effect.

It is known that the energy dissipation and, accordingly, stress hysteresis determine the coefficient of performance (COP). COP is used to classify the EC properties of materials in terms of application efficiency. This coefficient is equal to the ratio of the useful thermal energy obtained from an endothermic reaction of a sample and the environment during cooling to the energy dissipation characterizing the input work in the loading/unloading cycles [32,33]:

$$\text{COP} = \frac{C_p \Delta T_{ad}}{\frac{1}{\rho} \oint \sigma d\varepsilon} \quad (6)$$

where $2|\Delta G_{dis}| = \frac{1}{\rho} \oint \sigma d\varepsilon$ is the energy dissipation in the loading/unloading cycle.

Figure 9 shows the temperature dependence of the COP in the as-grown and aged $\text{Ni}_{54}\text{Fe}_{19}\text{Ga}_{27}$ crystals. It can be seen that high energy dissipation in the cycle and small specific heat capacity C_p (Table 1) lead to a significant decrease in the COP in the aged crystals compared with the as-grown ones. In the crystals aged at 773 K, the maximum COP reaches 10.6 and remains constant in a wide temperature range from 290 to 425 K. In the crystals aged at 1373 K, the maximum COP goes down and equals to 7.7. The maximum COP remains constant in a narrower temperature range from 313 to 400 K in these crystals. Nevertheless, the COP in the [001]-oriented $\text{Ni}_{54}\text{Fe}_{19}\text{Ga}_{27}$ crystals aged at 773 K for 1 h is comparable to that obtained earlier in copper alloys (CuAlMn, CuZnAl) and some ferromagnetic NiMnSn, NiMnInCo, and NiFeGaCo SMAs [1,34]. A wide range of operating temperatures and high cyclic stability of the SE and EC parameters allows us to conclude that the crystals aged at 773 K for 1 h have high potential for practical application along with the as-grown crystals.

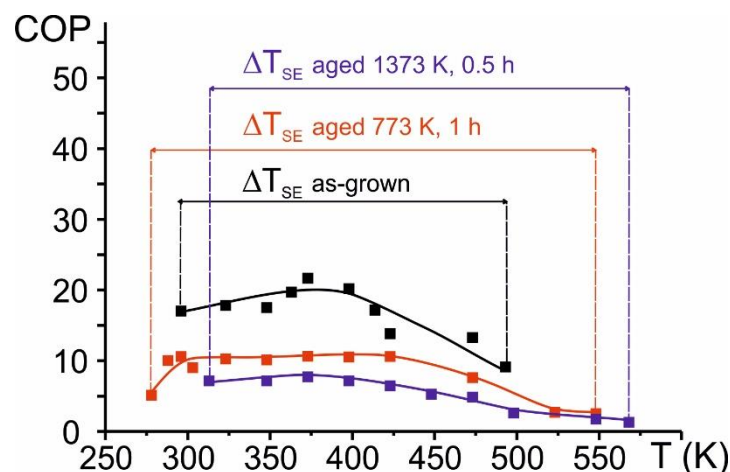


Figure 9. The temperature dependence of the COP in [001]-oriented $\text{Ni}_{54}\text{Fe}_{19}\text{Ga}_{27}$ single crystals.

5. Conclusions

The dependence of the EC effects on test temperature and particles size in the [001]-oriented aged $\text{Ni}_{54}\text{Fe}_{19}\text{Ga}_{27}$ single crystal undergoing $L_{21}(B2)$ -10M/14M- L_{10} martensitic transformations in compression have been studied. The main findings can be summarized as follows:

1. It has been shown that aging at 773 K for 1 h and aging at 1373 K for 0.5 h leads to the precipitation of semi-coherent γ' -phase particles up to 500 nm in size and incoherent γ' -phases particles from 5 to 35 microns in size, respectively. Precipitation of γ' -phases particles, which do not undergo transformations, results in a decrease in the transformation entropy changes ΔS^{A-M} (ΔS^{M-A}) for both forward and reverse L2₁(B2)-10M/14M-L1₀ martensitic transformations as compared with as-grown single crystals. Moreover, the specific heat capacity C_p also decreases by 54 J/(kgK) in the crystals aged at 773 K and by 70 J/(kgK) in the crystals aged at 1373 K as compared with the as-grown crystals;
2. The [001]-oriented Ni₅₄Fe₁₉Ga₂₇ single crystals aged at 773 K for 1 h exhibit the widest temperature range of the superelastic behavior and associated elastocaloric effect $\Delta T_{SE} = 270$ K with the maximum adiabatic cooling ΔT_{ad} up to 11.1 (± 0.5) K. The crystals with incoherent γ' -phase particles (aging at 1373 K, 0.5 h) show the operating temperature range of $\Delta T_{SE} = 255$ K with slightly smaller adiabatic cooling ΔT_{ad} below 9.7 (± 0.5) K. In contrast, the temperature range of the elastocaloric effect $\Delta T_{SE} = 195$ –200 K with the maximum adiabatic cooling ΔT_{ad} up to 10.9 (± 0.8) K is smaller in the as-grown crystals than in the aged ones;
3. The aged [001]-oriented Ni₅₄Fe₁₉Ga₂₇ single crystals demonstrate high cyclic stability: the adiabatic cooling ΔT_{ad} and loading/unloading curves do not depend on the number of operating cycles from 3 to 150 regardless of the particle size;
4. Wide stress hysteresis and low values of specific heat capacity C_p lead to the decrease in the coefficient of performance (COP = 10.6–7.7) in the aged crystals as compared with the as-grown crystals (COP is up to 21.7). Despite this feature, the wide operating temperature range of the EC effect and excellent reversibility of the EC performance make aged [001]-orientated Ni₅₄Fe₁₉Ga₂₇ single crystals a promising elastocaloric material.

Author Contributions: Conceptualization, E.Y.P. and Y.I.C.; methodology, Y.I.C., E.Y.P. and N.S.S.; validation, A.S.E., A.B.T. and E.E.T.; formal analysis, E.Y.P., N.S.S. and A.S.E.; investigation, E.I.Y., A.I.T. and I.D.K.; resources, E.Y.P. and Y.I.C.; writing—original draft preparation, E.I.Y.; writing—review and editing, E.Y.P. and Y.I.C.; visualization, E.I.Y.; supervision, E.Y.P. and Y.I.C.; project administration, A.S.E.; and funding acquisition, E.Y.P. All authors have read and agreed to the published version of the manuscript.

Funding: This research was funded by Russian Science Foundation, project 20-19-00153.

Institutional Review Board Statement: Not applicable.

Informed Consent Statement: Not applicable.

Data Availability Statement: The data used in this article are presented in the manuscript.

Conflicts of Interest: The authors declare no conflict of interest.

References

1. Qian, S.; Geng, Y.; Wang, Y.; Ling, J.; Hwang, Y.; Radermacher, R.; Takeuchi, I.; Cui, J. A review of elastocaloric cooling: Materials, cycles and system integrations. *Int. J. Refrig.* **2016**, *64*, 1–19. [[CrossRef](#)]
2. Chauhan, A.; Patel, S.; Vaish, R.; Bowen, C.R. A review and analysis of the elastocaloric effect for solid state refrigeration devices: Challenges and opportunities. *MRS Energy Sustain. Rev. J.* **2015**, *2*, E16. [[CrossRef](#)]
3. Cong, D.; Xiong, W.; Planes, A.; Ren, Y.; Manosa, L.; Cao, P.; Nie, Z.; Sun, X.; Yang, Z.; Hong, X.; et al. Colossal Elastocaloric Effect in Ferroelastic Ni-Mn-Ti Alloys. *Phys. Rev. Lett.* **2019**, *122*, 255703. [[CrossRef](#)]
4. Masdeu, F.; Pons, J.; Torrens-Serra, J.; Chumlyakov, Y.; Cesari, E. Superelastic behavior and elastocaloric effect in Ni_{51.5}Fe_{21.5}Ga_{27.0} ferromagnetic shape memory single crystal under compression. *Mater. Sci. Eng. A* **2022**, *833*, 142362. [[CrossRef](#)]
5. Xiao, F.; Jin, M.; Liu, J.; Jin, X. Elastocaloric effect in Ni₅₀Fe₁₉Ga₂₇Co₄ single crystals. *Acta Mater.* **2015**, *96*, 292–300. [[CrossRef](#)]
6. Wu, Y.; Ertekin, E.; Sehitoglu, H. Elastocaloric cooling capacity of shape memory alloys—Role of deformation temperatures, mechanical cycling, stress hysteresis and inhomogeneity of transformation. *Acta Mater.* **2017**, *135*, 158–176. [[CrossRef](#)]
7. Li, Y.; Zhao, D.; Liu, J. Giant and reversible roomtemperature elastocaloric effect in a single-crystalline Ni-Fe-Ga magnetic shape memory alloy. *Sci. Rep.* **2016**, *6*, 25500. [[CrossRef](#)]
8. Santamarta, R.; Font, J.; Muntasell, J.; Masdeu, F.; Pons, J.; Cesari, E.; Dutkiewicz, J. Effect of ageing on the martensitic transformation of Ni-Fe-Ga alloys. *Scr. Mater.* **2006**, *54*, 1105–1109. [[CrossRef](#)]

9. Chumlyakov, Y.I.; Kireeva, I.V.; Panchenko, E.Y.; Kirillov, V.A.; Timofeeva, E.E.; Kretinina, I.V.; Danil'son, Y.N.; Karaman, I.; Maier, H.; Cesari, E. Thermoelastic martensitic transformations in single crystals with disperse particles. *Russ. Phys. J.* **2012**, *54*, 937–950. [[CrossRef](#)]
10. Vetoshkina, N.; Panchenko, E.; Timofeeva, E.; Chumlyakov, Y.; Surikov, N.; Osipovich, K.; Maier, H. Effect of ageing on the cyclic stability of superelasticity in [001]-oriented Ni₄₉Fe₁₈Ga₂₇Co₆ single crystals in compression. *Mater. Today Proc.* **2017**, *4*, 4797–4801. [[CrossRef](#)]
11. Dadda, J.; Maier, H.J.; Karaman, I.; Chumlyakov, Y.I. Cyclic deformation and austenite stabilization in Co₃₅Ni₃₅Al₃₀ single crystalline high-temperature shape memory alloys. *Acta Mater.* **2009**, *57*, 6123–6134. [[CrossRef](#)]
12. Eftifeeva, A.; Panchenko, E.; Chumlyakov, Y.; Yanushonite, E.; Gerstein, G.; Maier, H.J. Compressive response of high-strength [001]-oriented single crystals of a Co₃₅Ni₃₅Al₃₀ shape memory alloy. *J. Alloys Compd.* **2019**, *787*, 963–971. [[CrossRef](#)]
13. Chumlyakov, Y.I.; Kireeva, I.V.; Panchenko, E.Y.; Timofeeva, E.E.; Kretinina, I.V.; Kuts, O.A. Physics of thermoelastic martensitic transformation in high-strength single crystals. *Mater. Sci. Found.* **2015**, *81–82*, 107–174. [[CrossRef](#)]
14. Zhao, D.; Xiao, F.; Nie, Z.; Cong, D.; Sun, W.; Liu, J. Burst-like superelasticity and elastocaloric effect in [011] oriented Ni₅₀Fe₁₉Ga₂₇Co₄ single crystals. *Scr. Mater.* **2018**, *149*, 6–10. [[CrossRef](#)]
15. Timofeeva, E.E.; Panchenko, E.Y.; Vetoshkina, N.G.; Chumlyakov, Y.I.; Tagiltsev, A.I.; Eftifeeva, A.S.; Maier, H. The mechanism of orientation dependence of cyclic stability of superelasticity in NiFeGaCo single crystals under compression. *Russ. Phys. J.* **2016**, *59*, 1251–1260. [[CrossRef](#)]
16. Larchenkova, N.G.; Panchenko, E.Y.; Timofeeva, E.E.; Tagiltsev, A.I.; Chumlyakov, Y.I. Cyclic stability of superelasticity in [001]-oriented stress-free and stress-assisted aged Ni₄₉Fe₁₈Ga₂₇Co₆ single crystals. *AIP Conf. Proc.* **2018**, *2051*, 020166. [[CrossRef](#)]
17. Eftifeeva, A.; Panchenko, E.; Yanushonite, E.; Kurlevskaya, I.; Timofeeva, E.; Tokhmetova, A.; Surikov, N.; Tagiltsev, A.; Chumlyakov, Y. Superelasticity and elastocaloric cooling capacity in stress-induced martensite aged [001]_A-oriented Ni₅₄Fe₁₉Ga₂₇ single crystals. *Mater. Sci. Eng. A* **2022**, in press.
18. Hohne, G.W.H.; Hemminger, W.; Flammersheim, H.-J. *Differential Scanning Calorimetry: An Introduction for Practitioners*; Springer: New York, NY, USA, 1996; p. 217.
19. Bolgar, M.K.; Daroczi, L.; Toth, L.Z.; Timofeeva, E.E.; Panchenko, E.Y.; Chumlyakov, Y.I.; Beke, D.L. Effect of g precipitates on thermal and acoustic noises emitted during austenite/martensite transformation in NiFeGaCo single crystals. *J. Alloys Compd.* **2017**, *705*, 840–848. [[CrossRef](#)]
20. Oikawa, K.; Ota, T.; Ohmori, T.; Tanaka, Y.; Morito, H.; Fujita, A.; Kainuma, R.; Fukamichi, K.; Ishida, K. Magnetic and martensitic phase transitions in ferromagnetic Ni-Ga-Fe shape memory alloys. *Appl. Phys. Lett.* **2002**, *81*, 5201–5203. [[CrossRef](#)]
21. Imano, Y.; Omori, T.; Oikawa, K.; Sutou, Y.; Kainuma, R.; Ishida, K. Martensitic and magnetic transformations of Ni-Ga-Fe-Co ferromagnetic shape memory alloys. *Mater. Sci. Eng. A* **2006**, *438–440*, 970–973. [[CrossRef](#)]
22. Picornell, C.; Pons, J.; Cesari, E.; Dutkiewicz, J. Thermal characteristics of Ni-Fe-Ga-Mn and Ni-Fe-Ga-Co ferromagnetic shape memory alloys. *Intermetallics* **2008**, *16*, 751–757. [[CrossRef](#)]
23. Sutou, Y.; Kamiya, N.; Omori, T.; Kainuma, R.; Ishida, K.; Oikawa, K. Stress-strain characteristics in Ni-Ga-Fe ferromagnetic shape memory alloys. *Appl. Phys. Lett.* **2004**, *84*, 1275–1277. [[CrossRef](#)]
24. Hamilton, R.F.; Sehitoglu, H.; Efstathiou, C.; Maier, H.J. Inter-martensitic transitions in Ni-Fe-Ga single crystals. *Acta Mater.* **2007**, *55*, 4867–4876. [[CrossRef](#)]
25. Panchenko, E.; Chumlyakov, Y.; Maier, H.J.; Timofeeva, E.; Karaman, I. Tension/compression asymmetry of functional properties in [001]-oriented ferromagnetic NiFeGaCo single crystals. *Intermetallics* **2010**, *18*, 2458–2463. [[CrossRef](#)]
26. Bruno, N.M.; Karaman, I.; Chumlyakov, Y.I. Orientation dependence of the elastocaloric effect in Ni₅₄Fe₁₉Ga₂₇ ferromagnetic shape memory alloy. *Phys. Status Solidi B* **2018**, *255*, 1700437. [[CrossRef](#)]
27. Mañosa, L.; Planes, A. Materials with giant mechanocaloric effects: Cooling by strength. *Adv. Mater.* **2017**, *29*, 1603607. [[CrossRef](#)]
28. Beke, D.L.; Daróczy, L.; Elrasasi, T.Y. Determination of elastic and dissipative energy contributions to martensitic phase transformation in shape memory alloys. In *Shape Memory Alloys—Processing, Characterization and Applications*; IntechOpen: London, UK, 2013. [[CrossRef](#)]
29. Chumlyakov, Y.I.; Kireeva, I.V.; Pobedennaya, P.; Krooß, P.; Niendorf, T. Rubber-like behaviour and superelasticity of [001]-oriented FeNiCoAlNb single crystals containing γ - and β -phase particles. *J. Alloys Compd.* **2021**, *856*, 158158. [[CrossRef](#)]
30. Li, P.; Karaca, H.E.; Chumlyakov, Y.I. Orientation dependent compression behavior of Co₃₅Ni₃₅Al₃₀ single crystals. *J. Alloys Compd.* **2017**, *718*, 326–334. [[CrossRef](#)]
31. Gall, K.; Maier, H.J. Cyclic deformation mechanisms in precipitated NiTi shape memory alloys. *Acta Mater.* **2002**, *50*, 4643–4657. [[CrossRef](#)]
32. Tusek, J.; Engelbrecht, K.; Manosa, L.; Vives, E.; Pruds, N. Understanding the thermodynamic properties of the elastocaloric effect through experimentation and modeling. *Shap. Mem. Superelasticity* **2016**, *2*, 317–329. [[CrossRef](#)]
33. Yang, Z.; Cong, D.Y.; Sun, X.M.; Nie, Z.N.; Wang, Y.D. Enhanced cyclability of elastocaloric effect in born-microalloyed Ni-Mn-In magnetic shape memory alloys. *Acta Mater.* **2017**, *127*, 33–42. [[CrossRef](#)]
34. Guo, J.; Wei, Z.; Shen, Y.; Zhang, Y.; Li, J.; Hou, X.; Liu, J. Low-temperature superelasticity and elastocaloric effect in textured Ni-Mn-Ga-Cu shape memory alloys. *Scr. Mater.* **2020**, *185*, 56–60. [[CrossRef](#)]